JOURNAL OF GEOPHYSICAL RESEARCH, VOL. 89, NO. A9, PAGES 7357-7366, SEPTEMBER 1, 1984

ACCELERATION OF LITHIUM TEST IONS IN THE QUIET TIME GEOMAGNETIC TAIL

Sandra C. Chapman and S. W. H. Cowley

The Blackett Laboratory, Imperial College of Science and Technology, London

Abstract. One of the active experiments to be performed as part of the Active Magnetospheric Particle Tracer Explorers mission involves the release of lithium ions in the geomagnetic tail and their subsequent detection after earthward convection into the nightside outer ring current region. In this paper we have used the guiding center approximation to integrate ion trajectories in a simple two-dimensional model of the quiet time nightside magnetosphere in order to estimate expected ion properties at the latter location. Our principal conclusion is that under typical quiet time conditions these ions will predominantly form a field-aligned beam ($\sim 5° - 20°$ pitch angle) at energies from a few hundred eV to ~ 1 keV.

1. Introduction

A principal objective of the Active Magnetospheric Particle Tracer Explorers (AMPTE) spacecraft mission is the study of the chemical releases to be made by the ion release module (IRM) in the magnetospheric tail and solar wind, and the subsequent detection of the tracer ions by the charge composition explorer (CCE) after they have been transported by magnetospheric flows into the ring current region. The experiment of particular interest here is the lithium release to be made in the plasma sheet region near the center of the geomagnetic tail at a down-tail distance of $\sim 20\ R_E$. Such a release will result in the production of $\sim 10^{24}$ atoms of neutral lithium vapor which are expected to form initially a spherical cloud expanding at a speed ~ 4 km s^{-1}. This speed corresponds to an energy of ~ 1 eV per atom produced by the release chemistry. The atoms will then be photoionized by sunlight with a time constant of ~ 1 hour, seeding the magnetospheric plasma flowing through the neutral cloud with singly charged lithium ions. After two time constants or ~ 2 hours, when $\sim 85\%$ of the atoms have been ionized, the cloud will have expanded to a diameter of $\sim 10\ R_E$, comparable to the full thickness of the quiet time plasma sheet. Estimates of the typical lithium ion number density in the resulting seeded plasma are of the order of $\sim 10^{-5}$ cm^{-3} [Krimigis et al., 1982]. Since this represents a mass density which is much smaller than the ambient plasma density, the acceleration of these ions to the local flow speed is not expected to extract significant energy or momentum from the flow. The ions may thus be regarded as test particles injected into the ambient plasma.

In this paper we shall present some results of a theoretical study of ion behavior in the nightside magnetosphere. The objective of the study is to understand some of the significant factors which will determine the properties of the released ions on arrival from the tail in the nightside ring current region. To do this we have integrated trajectories of test ions in a simple model electromagnetic field using guiding center theory, and have followed the ions as they are convected from their release points in the tail into the inner dipole-dominated magnetosphere. Here, in section 2, we describe the model electromagnetic field we have used, while in section 3 we discuss the integration of guiding center trajectories in this model field. In section 4 some sample results are presented, and their significance for the AMPTE mission is finally discussed in section 5.

Paper number 4A0487.
0148-0227/84/004A-0487$05.00

2. The Model Electromagnetic Field

In this section we will briefly describe the important features of the electromagnetic field which we have used for the trajectory integration studies. It should be emphasized from the outset that our objective here has been to produce only the simplest reasonable model field having the characteristics required for our study, and not to derive a complex and detailed model of the near-earth nightside magnetosphere, which for our purposes is unecessary. The major simplification introduced is that the magnetic field is taken to be two dimensional and planar, and hence derivable from a vector potential $A_y(x,z)\hat{y}$, using usual magnetospheric coordinates. This choice greatly simplifies the analysis of the trajectories as described in the next section, without sacrificing any of the essential physics.

The vector potential is taken to be the sum of two terms, the first being that of a line dipole located at the origin and the second representing the field due to the magnetotail current.

$$A_y = -\frac{Kx}{(x^2 + z^2)} + CF(x)\, e^{Ax} \cos kz \qquad (1)$$

where

$$F(x) = \frac{(\frac{x}{p})^2}{(1 + (\frac{x}{p})^2)}$$

The resulting divergence-free magnetic field components are

$$B_x(x,z) = -\frac{\partial A_y}{\partial z} = \frac{2Kxz}{(x^2+z^2)^2} + k\, CF(x) e^{Ax} \sin kz \qquad (2)$$

and

$$B_z(x,z) = \frac{\partial A_y}{\partial x}$$

$$= \frac{K(x^2-z^2)}{(x^2+z^2)^2} + Ce^{Ax}[AF(x) + \frac{2(\frac{x}{p^2})}{(1 + (\frac{x}{p})^2)^2}] \cos kz \qquad (3)$$

If we consider first the B_x component produced by the tail current it can be seen that at a given down-tail distance x the field varies as sin kz from zero at the center of the plasma sheet to a maximum value dependent on x at $z = z_m = \pi/(2k)$. The location $z = z_m$ thus represents the half thickness of the plasma sheet, which in this model is independent of down-tail distance and is taken to be 6 R_E in the numerical values given below. The tail current is thus broadly distributed (as cos kz) over a layer $\sim$ 12 R_E wide, as seems reasonable for the thick, quiet time plasma sheet. The tail field and current structure repeats periodically with z in the model due to the sinusoidal dependence, of course, and so we confine our attention here to the range $|z| \lesssim z_m$ outside of which the behavior is unphysical.

Turning now to the variation of B_x with down-tail distance x at a given z, it can be seen from (2) that in the tail proper (where $|x| >> p$ so that $F(x) \simeq 1$) there is a slow exponential increase in the field magnitude on scale length A^{-1} as the earth (i.e., the line dipole) is approached from large distances. This behavior changes near the dipole due to the F(x) factor which results in the B_x field due to the tail current then falling to zero at $x = 0$ on a scale determined by the length p, this representing the termination of the tail current and ring current systems in the near-earth nightside magnetosphere. These variations in B_x are mirrored in the behavior of B_z arising from the tail current term, which is positive and proportional to A in the tail proper ($|x| >> p$), reversing to become negative in the near-earth region due to the termination and closure of the tail field system (second term in the square brackets in (3)). In the absence of the dipole term, the tail current would produce distended closed field line loops wholly confined within the rectangle defined by $|z| \lesssim z_m$ and $0 \lesssim x \lesssim -\infty$, noting that B_z varies as cos kz and hence goes to zero at $|z| = z_m$.

In assigning values to the parameters in (1) particular attention has been paid to two requirements. The first is that there should be a smooth transition from taillike distended field lines at large $|x|$ to dipole-dominated behavior at small $|x|$. The second is that the magnetotail field in the vicinity of the lithium release at $x \sim -20$ R_E should be as realistic as possible, since it is found that the initial interaction of the test ions with the current sheet is crucial in determining their properties. We have therefore taken the line dipole strength such as to give a contribution to the B_z field at $z = 0$ similar to the earth's dipole at $x \simeq -20$ R_E (3.75 nT in the model). However since the field strength for a line dipole varies as the inverse square of the distance rather than as the inverse cube, this means that the magnitude of the dipole field inside this location will be rather less than actual magnetospheric values. This simply has the effect of reducing the down-tail distance of the transition from dipole to tail field dominance, and is not crucial to our study since ion motion in this regime may be expected to conserve the second adiabatic invariant J as well as the first, allowing us to use our results to estimate values which are appropriate to a more realistic field.

The parameter values taken were then as follows, where the units are such that if x and z are in R_E in (1) to (3) then $\underline{B}$ is in nT and A_y in nT R_E:

$$K = 1500 \text{ nT } R_E^2 \qquad A = 0.011 \ R_E^{-1}$$

$$C = \frac{264}{\pi} \simeq 84.03 \text{ nT } R_E$$

$$k = \frac{\pi}{12} \simeq 0.262 \ R_E^{-1} \qquad p = 6 \ R_E$$

The properties of the resulting field in the region of interest are shown in Figures 1 and 2. The left-hand panel of Figure 1 shows the variation of B_z with down-tail distance at $z = 0$ (curve C), together with the contributions of the dipole (A) and the tail field (B) separately. The latter is negative in the region $|x| \lesssim 18$ R_E due to the termination factor F(x), and is small but positive in the vicinity of $x \simeq -20$ R_E where the dipole term consequently dominates giving a net $B_z \simeq 4$ nT in this region. The total B_z field decreases smoothly with increasing distance from the dipole as required. The right-hand panel in Figure 1 shows the variation of B_x and B_z versus z at $x = -20$ R_E. While B_z is mainly due to the dipole term at this distance, B_x is dominated by the tail current contribution and rises to a value of $\sim$ 18.1 nT at the edge of the plasma sheet at $|z| = 6$ R_E. These values for the fields at $x \simeq -20$ R_E are in good agreement with the quiet time values published [e.g., Behannon, 1968, 1970; Mihalov et al., 1968; Fairfield, 1979]. In Figure 2 we show field lines of the model field given by the contours A_y = constant. Lines are shown at equal intervals of A_y so that their spacing gives a measure of field strength. The dashed lines show field lines with the same A_y values which would result from the dipole term alone, in order to give an indication of the distortion due to the tail current system. For a line dipole these field lines are circles intersecting the origin. It can be seen that the transition from dipole- to tail-dominated fields takes place at a distance of $\sim$ 10 R_E.

Finally, the other essential ingredient in our model is a cross-tail electric field E_y associated with earthward convection in the plasma sheet. In our two-dimensional system this field must be uniform. The value of E_y in the model will be discussed further in the next section, but it may be noted here that typical transpolar potential rops of $\sim$ 50 kV measured by low-altitude spacecraft [e.g., Reiff et al., 1981] translate to $E_y \sim 0.2$ mV m^{-1} in a $\sim$ 40-R_E diameter tail.

3. Test Ion Trajectory Integration

In this section we will describe some general features of particle behavior in our model field, before describing the numerical results in section 4. As indicated in the introduction, we have used the guiding center approximation to compute efficiently the particle motion between the tail and the quasi-dipolar ring current region. The validity of this approximation for lithium ions in our model field will be discussed together with the numerical results in the next section.

In the guiding center approximation the particle motion is taken to consist of a series of terms of

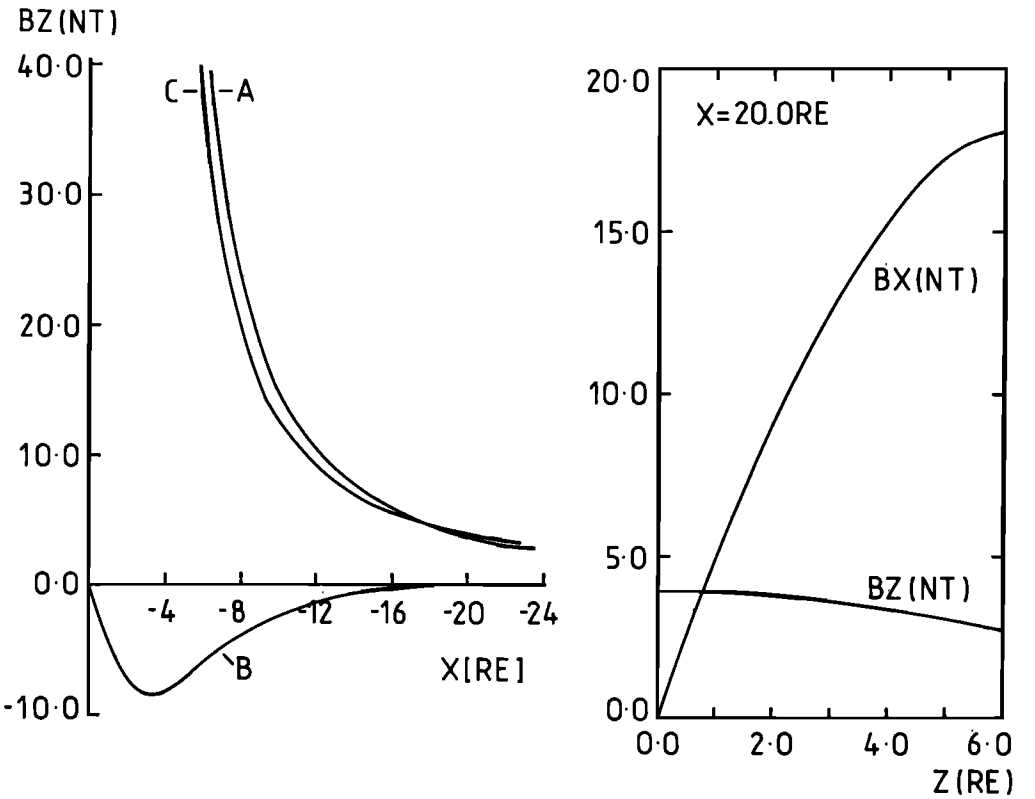

Fig. 1. The left-hand panel shows the variation with down-tail distance of the z component of the model magnetic field at the tail center plane (z = 0). Curve A represents the contribution of the dipole term, curve B the contribution of the tail current term and the total resultant B_z field is curve C. The right-hand panel shows the variation of the x and z components of the model field (in nT) at a distance of x = - 20 R_E, with distance z (R_E) from the center plane.

decreasing magnitude, the smallness parameter of which may be considered to be the mass to charge ratio m/q of the particle [Northrop, 1963]. The zero-order motion is that appropriate to a uniform and constant electromagnetic field with $\underline{E}.\underline{B} = 0$, and consists of gyration about the magnetic field lines at speed $v_\perp$, giving no net translation, together with steady motion parallel and

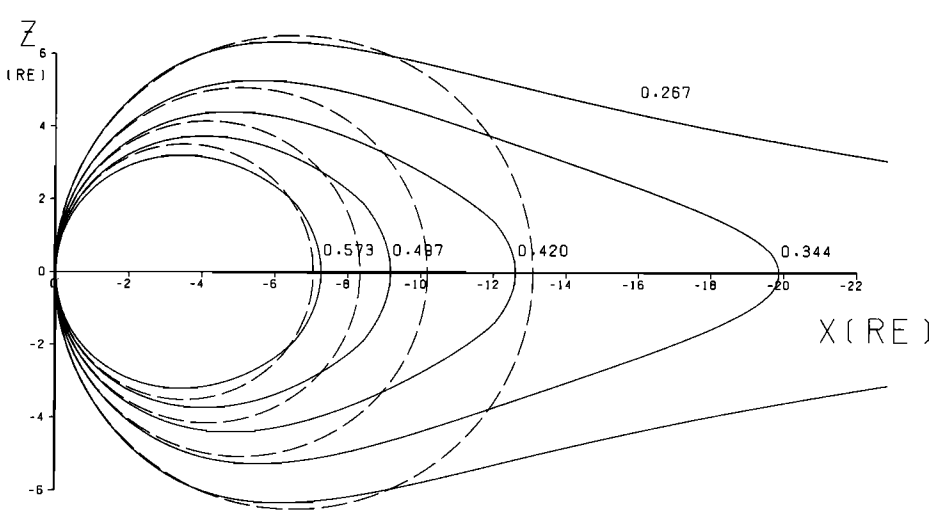

Fig. 2. Contours of constant vector potential for the field model in the x - z plane. Distances are in units of R_E. The solid lines denote field lines given by contours of constant A_y at equal intervals. Numbers adjacent to each contour give the corresponding magnitude of A_y in units of nT R_E. The dashed lines indicate contours with the same A_y values derived from the dipole term of the model field alone.

perpendicular to $\underline{B}$ given by $v_{\parallel}\underline{b}$ and $\underline{U_E}$, where $\underline{b}$ is the unit vector along $\underline{B}$ and $\underline{U_E}$ is the $\underline{E} \wedge \underline{B}/B^2$ drift. The first-order motion proportional to m/q then consists (in the absence of gravity, $E_{\parallel}$, etc.) of drifts related to the first time and space derivatives of the electromagnetic field. In our case there are three terms, the gradient and curvature magnetic drifts, together with a drift related to the spatial variation of $\underline{U_E}$. In the two-dimensional field used here, however, we have the special property that the zero-order steady motions $v_{\parallel}\underline{b}$ and $\underline{U_E}$ are confined to the planes parallel to the x - z plane containing the field lines, while the first-order drifts have only cross-tail y components perpendicular to these planes. The guiding center motion projected onto the x - z plane may then be obtained by integration of the following equations:

$$\frac{d\underline{r}}{dt} = \underline{U_E} + v_{\parallel}\underline{b} \tag{4}$$

where $\underline{r}$ is the position vector of the guiding center and $v_{\parallel}$ is determined from [Northrop, 1963]

$$\frac{dv_{\parallel}}{dt} = -\frac{\mu}{m}\frac{\partial B}{\partial s} + \underline{U_E} \cdot \frac{d\underline{b}}{dt} \tag{5}$$

In (5) s is distance along the magnetic field lines and the magnetic moment $\mu = mv_{\perp}^2/2B$ is an invariant of the motion which determines $v_{\perp}$ on the trajectory. It should be noted that the x - z motion is independent of the particle mass or charge for given initial conditions $\underline{r}$ and $\underline{v} = (v_{\parallel}, v_{\perp})$, provided, of course, that the guiding center approximation remains valid. The y displacement of the particle due to the first-order drifts depends on m/q, however, and is given by

$$qv_D E_y = \frac{m}{2}\frac{d}{dt}(v_{\perp}^2 + v_{\parallel}^2 + U_E^2) \tag{6}$$

where v_D is the total drift speed in the y direction. It can be seen from (6) that the particle displacement in the direction of the electric field due to these drifts is just such as to account for the changes in kinetic energy of the zeroth-order motion. The first-order drifts do not, therefore, have to be integrated explicity, the y displacement from the initial value being given by the change in the total (gyrophase averaged) zeroth-order kinetic energy. For the lithium ions considered here we find in the next section that energy changes in the tail are typically of the order of a few hundred eV, rising to $\sim$ 1 keV during inward convection into the ring current region. For typical values $E_y \sim 1$ kV R_E^{-1} the cross-system displacements are therefore small, $\lesssim 1\ R_E$.

Another exact integral of the motion may be obtained from (4), in this case relating to the cross-field drift parallel to the x - z plane. It is readily shown that the expression for the rate of change of A_y at the guiding center may be integrated to yield

$$A_y(t) = A_y(t_0) + (t - t_0)E_y \tag{7}$$

This equation expresses the linear increase with time of the zeroth-order canonical y momentum of the particle due to E_y, it being remembered that the mean speed v_y itself is a first-order quantity. Equation (7) determines the field line (A_y value) on which the particle will be located at any time in terms of initial values, but the position on that field line can only be determined by simultaneous integration of (4) and (5). In practice the trajectories presented in the next section have been determined by direct integration of (4) and (5), and exact integral (7) has been used only to verify the accuracy of this integration. One interesting general consequence of (7) is that all particles whose guiding centers lie on a particular field line (projected onto the x - z plane) at a particular time will for all time have their guiding centers (projected onto the x - z plane) joined by a field line, independent of particle energy, mass or charge. In this configuration, therefore, an exact and extended meaning can be given to the "moving field line" picture.

Having now discussed the general properties of particle motion in our model field we now turn to consider the specific properties of the lithium test ions, and begin by examining the initial conditions just after photoionization. An important simplification may be introduced by noting that the initial ion velocity arising from the "thermal" velocity of the "parent" atom will generally be quite small compared with the local plasma flow speed $|\underline{U_E}|$. The thermal atom speed is expected to be ~ 4 km s^{-1}, compared with typical flow speeds at down-tail distances $\sim 20\ R_E$ of ~ 10 km s^{-1} at the outer edge of the plasma sheet, rising to ~ 50 km s^{-1} at the center plane (taking, e.g., our model field and $E_y \simeq 0.2$ mV m^{-1}). We can therefore to a reasonable approximation neglect the initial atomic velocity and take the ions as being created at rest in crossed electric and magnetic fields. The resulting initial motion is hence cycloidal, corresponding to initial ion velocity components $v_{\parallel} = 0$ and $v_{\perp} = |\underline{U_E}| = E_y/B$.

An important consequence of this approximation is that the guiding center trajectory of a test ion in the x,z plane created at a particular point in the field is actually independent of the electromagnetic field magnitudes chosen. Suppose, for example, we take an electromagnetic field E_y and $\underline{B}(x,z)$, and start a particle at position $\underline{r}_0 = (x_0, 0, z_0)$ with $v_{\parallel} = v_{\parallel 0}$ and $v_{\perp} = v_{\perp 0}$ such that the resulting trajectory is $\underline{r}(t) = (x(t), y(t), z(t))$. We now change the field magnitudes to $E_y' = \alpha E_y$ and $\underline{B}'(x,z) = \beta\underline{B}(x,z)$ such that the $\underline{E} \wedge \underline{B}$ drift scales according to $\underline{U_E}' = (\alpha/\beta)\underline{U_E}$ and start the particle at the same position with $v'_{\parallel 0} = (\alpha/\beta)v_{\parallel 0}$ and $v'_{\perp 0} = (\alpha/\beta)v_{\perp 0}$. It is then easily shown that the trajectory satisfying (4), (5) and (6) is given by

$$\underline{r}'(t) = \left(x\left(\frac{\alpha}{\beta}t\right), \frac{\alpha}{\beta^2}y\left(\frac{\alpha}{\beta}t\right), z\left(\frac{\alpha}{\beta}t\right)\right)$$

i.e., the x - z trajectory is the same as before but is simply traced out at a different rate. It is to be emphasized that this result relies on the assumption that the initial speeds $v_{\parallel 0}'$ and $v_{\perp 0}'$ scale according to the scaling of the electric drift $\underline{U_E}'$. However, this is just the situation encountered in this problem where the initial conditions are taken to be $v_{\parallel} = 0$ and $v_{\perp} = |\underline{U_E}|$.

In the numerical results to be given in the next section, therefore, the trajectory traces in the x - z plane are wholly independent of the magnitudes of the fields. For convenience,

velocities have been normalized to the electric field drift velocity at any point in the model field where B = 20 nT. If a typical value $E_y = 0.2$ mV m^{-1} is then taken for the electric field, the unit of speed is just 10 km s^{-1}. For instance, at the plasma sheet edge where B ≃ 18.1 nT in the model field, the normalized drift speed is $|U_E^*| \simeq 20/18.1 \simeq 1.11$, and if we then take $E_y = 0.2$ mV m^{-1}, the drift speed is just 11.1 km s^{-1}. This scaling will be used to illustrate our normalized results in the next section but values appropriate to other choices of E_y and absolute $\underline{B}$ field magnitude may be readily calculated. We have also normalized lengths to the plasma sheet scale thickness k^{-1} (see equation (1)), which, according to the values in section 2 has a typical value $12/\pi \simeq 3.82$ R_E. Times have thus been normalized to the unit $(k|U_{E0}|)^{-1}$ which for the values given above and taking $R_E \simeq 6400$ km is an interval of ∿ 41 min. In the next section all normalized quantities will be indicated by an asterisk.

4. Numerical Results

Having normalized the equations of motion (4) and (5) according to the above scheme we have then integrated them with a fourth-order Runge-Kutte scheme, using exact integral (7) as a check on accuracy. The time step was taken sufficiently small that the latter was satisfied to within 1% over the entire trajectory. Particles were started with the initial conditions described in section 3 at a down-tail distance $x^* \simeq -5.24$ (corresponding to $x = -20$ R_E with the above scaling) and at various heights z^* through the full thickness of the plasma sheet $0 \lesssim z^* \lesssim \pi/2$ (corresponding to $0 \lesssim z \lesssim 6$ R_E), it being remembered that the neutral lithium cloud will have expanded to a diameter of ∿ 10 R_E in the ∿ 2-hour interval during which significant ion production occurs. Here we will now present some sample results which show how the behavior and acceleration of the test ions depend on where the ions are created within the plasma sheet.

The majority of the ions will be created away from the immediate vicinity of the plasma sheet center so that $|B_x| \gg B_z$ at the initial point (see Figure 1, right-hand panel). All such ions behave in qualitatively the same way and are exemplified here by the trajectory shown in Figure 3 which was started halfway between the center and the outer edge of the plasma sheet (i.e., at $x^* \simeq -5.24$, $z^* \simeq 0.79$, or $x = -20$ R_E, $z = 3$ R_E with the above scaling). In the upper panel of Figure 3 we show the trajectory in the x^*,z^* plane together with the field lines (dashed lines), while in the lower panel we show versus normalized time the particle pitch angle (defined by $\tan^{-1} v_\perp^*/|v_\parallel^*|$ so that it always lies in the range 0° to 90°), the normalized velocity components $v_\perp^*$ and $v_\parallel^*$, and also, at the bottom of the figure, the normalized x^* location of the particle which is shown to facilitate comparison with the trajectory trace.

At the point of creation the ion in Figure 3 has velocity components $v_\parallel^* = 0$ and $v_\perp^* = U_E^* \simeq 1.53$, so that as for all the particles considered here the initial pitch angle is 90°. With the "typical" velocity scaling of section 3 this $v_\perp^*$ value corresponds to ∿ 15.3 km s^{-1}, associated with an initial lithium ion energy of ∿ 8.6 eV. From the initial point the ion slowly $\underline{E} \wedge \underline{B}$ drifts toward the center plane, remaining at a large pitch angle until $|B_x|$ at the gyrocenter decreases to approach B_z in magnitude so that the field direction starts to change appreciably. The particle then becomes strongly accelerated along the field direction due to the $\underline{U_E} \cdot d\underline{b}/dt$ term in (5), and the pitch angle falls to small values. On crossing the center plane $v_\parallel^*$ is found to have increased to a value approximately equal to U_E^* at that location ($v_\parallel^* \simeq 4.8$; $U_E^* \simeq 4.5$), subsequently increasing to roughly twice that value before leaving the central region on the other side of the sheet. For the typical velocity scaling in section 3 the total increase in $v_\parallel$ is ∿ 85 km s^{-1}, corresponding to a lithium ion energy of ∿ 260 eV. In its interaction with the weak field region at the sheet center, therefore, the ion is strongly accelerated along the field direction and emerges into the strong $|B_x|$ region on the other side of the current sheet as a field-aligned (∿ 8° pitch angle) particle.

This behavior can be readily understood by a frame transformation argument which is rigorous only when B_z is strictly uniform in the current sheet, but which applies to a good approximation in this problem, since B_z is only weakly spatially varying over the region where the ions have their first interaction with the central current sheet (see Figure 1). If in this region we transform to a frame moving earthward with the local equatorial electric drift speed $U_{E_C} = E_y/B_z$, then in this frame the electric field will be transformed to zero [de Hoffman and Teller, 1950; Speiser, 1965; Cowley, 1980]. Consequently in this frame the particle speed is constant, and the guiding center projected onto the x - z plane will move along a given field line (A_y contour) from one side of the current sheet to the other, the motion being symmetrical about the center plane. If the ion is created away from the immediate center of the current sheet where $|B_x| \gg B_z$, then since in the earth's frame the initial parallel speed is zero, in the transformed frame the parallel speed will be approximately the transformation velocity U_{E_C}. In either frame the initial perpendicular speed is $v_\perp = E_y/B$ where B is the total field strength at the point of creation, which is much larger than B_z. Consequently, while the initial ion pitch angle is 90° in the earth's frame, in the transformed frame the initial pitch angle is small (given by $\sin^{-1}(B_z/B)$), and the ion subsequently moves with a nearly constant field-aligned speed ∿ U_{E_C} from one side of the current sheet to the other. In the earth's frame such ions will thus be found to accelerate along the field to a speed $v_\parallel \simeq U_{E_C}$ (in the north-south direction) as they cross z = 0, and eventually to $v_\parallel \simeq 2\,U_{E_C}$ (directed toward the earth) as they move into the large $|B_x|$ region on the other side of the current sheet.

Following the field-aligned acceleration near the center plane the ion in Figure 3 moves toward the earth with nearly constant speed and mirrors at a field strength which would be reached at a radial distance of ∿ 5 R_E in the earth's three-dimensional dipole. In Figure 3, lower panel, the mirrorings are obvious from the 90° peaks in the pitch angle, corresponding to the peaks in $v_\perp^*$ and reversals in $v_\parallel^*$. The ion then returns to the center plane, but at a point displaced considerably earthward of the initial crossing, due to the

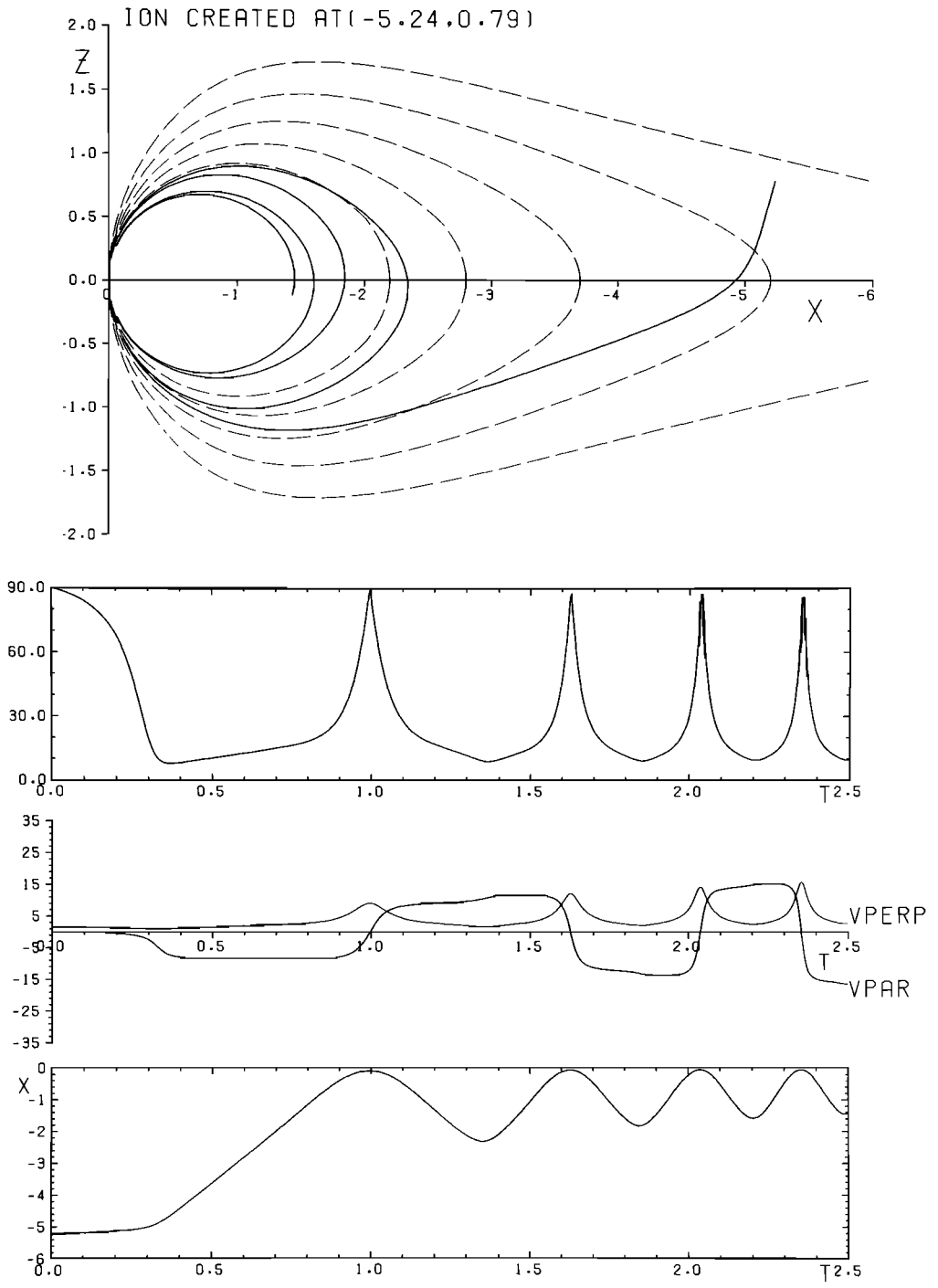

Fig. 3. The upper panel shows the guiding center trajectory of an ion in the model field projected onto the x - z plane. Distances are given as multiples of the plasma sheet scale thickness $k^{-1} \simeq 3.82\ R_E$. The ion was created halfway between the center plane and the current sheet edge at a down-tail distance of 20 R_E; its trajectory is marked by the solid line. The dashed lines denote the field lines as shown in the previous figure. In the lower panel the variation of the pitch angle and velocity components of the ion trajectory are plotted versus time. Time is expressed as multiples of the characteristic time which, for typical values, is $\sim$ 41 min. The upper plot shows the ion pitch angle defined as $\tan^{-1}(v_\perp/|v_\parallel|)$, which is hence always in the range 0° - 90°. The middle plot shows the ion velocity components expressed as multiples of the characteristic drift speed, which is typically 10 km s^{-1}. The x displacement of the ion, again in normalized units, is shown in the lower plot, to allow the quantities plotted here to be related to the trajectory in the upper panel.

continual inward convection during its motion to the mirror point and back again. During the second crossing a further increase in $v_{\parallel}^*$ occurs (near $T^* \simeq 1.35$), which is again approximately twice the local equatorial U_E drift speed in magnitude as expected in the above argument. Similar features occur at subsequent crossings, though becoming less pronounced as U_{E_C} decreases in the inner dipole-dominated field region. It should be noted that the equatorial pitch angle of the particle remains small as the energy increases during the inward transport. When the ion crosses the field line mapping to the equator at $x = -8\ R_E$ ($x^* \simeq -2.09$), in the vicinity of which it is planned to detect them with the CCE spacecraft, the particle speed has increased to $v^* = \sqrt{v_{\perp}^{*2} + v_{\parallel}^{*2}} = 12.2$, corresponding to ~ 120 km s^{-1} and an ion energy of ~ 540 eV with the typical scaling. The equatorial pitch angle (obtained from the local value at the field line crossing by transforming at constant energy and magnetic moment) is $\sim 9°$. Detailed analysis of the trajectory shows that the increase in $v_{\parallel}$ is quite well approximated by $v_{\parallel}L \approx$ constant following the first current sheet acceleration, where L is the field line length. Since the length of a field line which passes through the equator at a given distance from the dipole cannot be sensitively dependent on the field model, the above energy is probably a reasonable estimate of the expected lithium ion energy on arrival in the outer ring current region. The pitch angle estimate is probably too small, however, since $v_{\perp}$ is proportional to $\sqrt{B}$ by conservation of μ, and the equatorial field strength of the model field at $x = -8\ R_E$ is probably too low by a factor of ~ 2.5 as a result of using the line dipole. Increasing $v_{\perp}$ by the factor $\sqrt{2.5} \simeq 1.6$ would then lead to equatorial pitch angles of $\sim 14°$ instead of $\sim 9°$.

The type of behavior described above is valid for a majority of the release ions which are created in the region of the plasma sheet where $|B_x|$ is large compared with B_z. On arrival in the ring current region these particles will all have similar energies and small pitch angles, since they will all be accelerated to nearly the same field-aligned speed on first crossing the central current sheet (i.e., $v_{\parallel} \simeq 2E_y/B_z$). The pitch angle will slowly increase for particles created successively closer to the center plane, however, since $v_{\perp}$ is determined by the drift speed $U_E = E_y/B$ at the point of creation and subsequent conservation of μ.

For particles created very close to the plasma sheet center, however, such that $|B_x|$ is comparable to or smaller than B_z, $v_{\perp}$ is no longer small and the motion is then qualitatively different from that described above. This is readily seen by considering the particle created exactly at the center plane $z = 0$ (not illustrated). In this case the ion immediately on ionization acquires a speed E_y/B_z, but now in the perpendicular component $v_{\perp}$, rather than in $v_{\parallel}$ as for the above ions. The particle is subsequently convected earthward, remaining at 90° pitch angle in the equatorial plane, $v_{\perp}$ steadily increasing proportional to $\sqrt{B_z}$ by conservation of μ. For such an ion created at $x = -20\ R_E$ and convected to $-8\ R_E$ in our model field the normalized speeds are $v_{\perp}^* \simeq 5.1$ and 11.4 respectively, corresponding with the typical scaling to $v_{\perp} \simeq 50$ and 110 km s^{-1} and to energies of ~ 100 and ~ 500 eV. The latter value is again probably too low by a factor of ~ 2.5 for reasons given above: an energy of ~ 1 keV at $x = -8\ R_E$ would probably be a better estimate for a three-dimensional dipole field. It can be seen, however, that particles created near the center plane will arrive in the ring current region with energies similar to those created further away from the center, but with large rather than small pitch angles.

A trajectory exhibiting these properties is shown in Figure 4, in the same format as Figure 3. This ion is created at $x^* \simeq -5.24$ and $z^* = 0.11$ (i.e., $x = -20\ R_E$ and $z^* \simeq 0.42\ R_E$) where $B_x \approx B_z/2$, such that the initial speed $v_{\perp}^* \simeq 4.6$ is similar to the 90° pitch angle particle discussed above. Due to the large magnetic moment the ion no longer mirrors close to the dipole but remains confined near the equator. The field-aligned speed $v_{\parallel}^*$ is of similar magnitude to $v_{\perp}^*$ at the first crossing of the center plane, but does not change appreciably thereafter, whilst $v_{\perp}^*$ itself increases steadily with time from conservation of μ. As a consequence, the equatorial pitch angle slowly increases toward 90° during inward transport.

An intermediate trajectory in which both $v_{\perp}$ and $v_{\parallel}$ increase, and remain comparable in magnitude during the motion is shown in Figure 5. This ion starts at $x^* = -5.24$ and $z^* = 0.335$ (i.e., $x = -20\ R_E$, $z = 1.28\ R_E$) where $B_x \simeq 1.5\ B_z$. Although the motion is rather different in the three cases illustrated here it can be seen that the speeds on crossing a particular field line are not dissimilar.

An overall summary of our numerical results as they apply to the expected lithium ion properties on arrival in the quasi-dipolar ring current region is shown in Figure 6. Here we show the normalized speed $v^* = \sqrt{v_{\perp}^{*2} + v_{\parallel}^{*2}}$ and the equatorial pitch angle for ions on crossing the field line which maps to the equator at $x = -8\ R_E$ (i.e., $x^* \simeq -2.09$), plotted against the normalized distance from the plasma sheet center z^* at which they were created at $x = -20\ R_E$. Local velocity coordinates on crossing the specified ring current field were transformed to equatorial values using conservation of energy and μ. This procedure is meaningful if, as here, the particle speeds are large compared with the electric field drift speed on the field line (by a factor of ~ 10 in Figure 6). As indicated above, these results show explicitly that v^* does not depend strongly on initial z^*. The typical value $v^* \simeq 12$ corresponds to ~ 120 km s^{-1} with the usual scaling and hence to a typical energy of ~ 525 eV. On the other hand the particle pitch angle does depend sensitively on initial z^*, varying from 90° to $\sim 5°$ as z^* increases from zero (sheet center) to $\pi/2$ (sheet edge). Over most of this range, however, the resulting pitch angle is small and in the range $\sim 5° - 15°$.

The final topic which we need to discuss briefly here is the validity of the approximations employed in this work. The major approximation is, of course, the use of guiding center theory to describe the initial interaction of the ions with the central region of the current sheet. This theory is valid provided that the fractional change in the field experienced by the particle in its

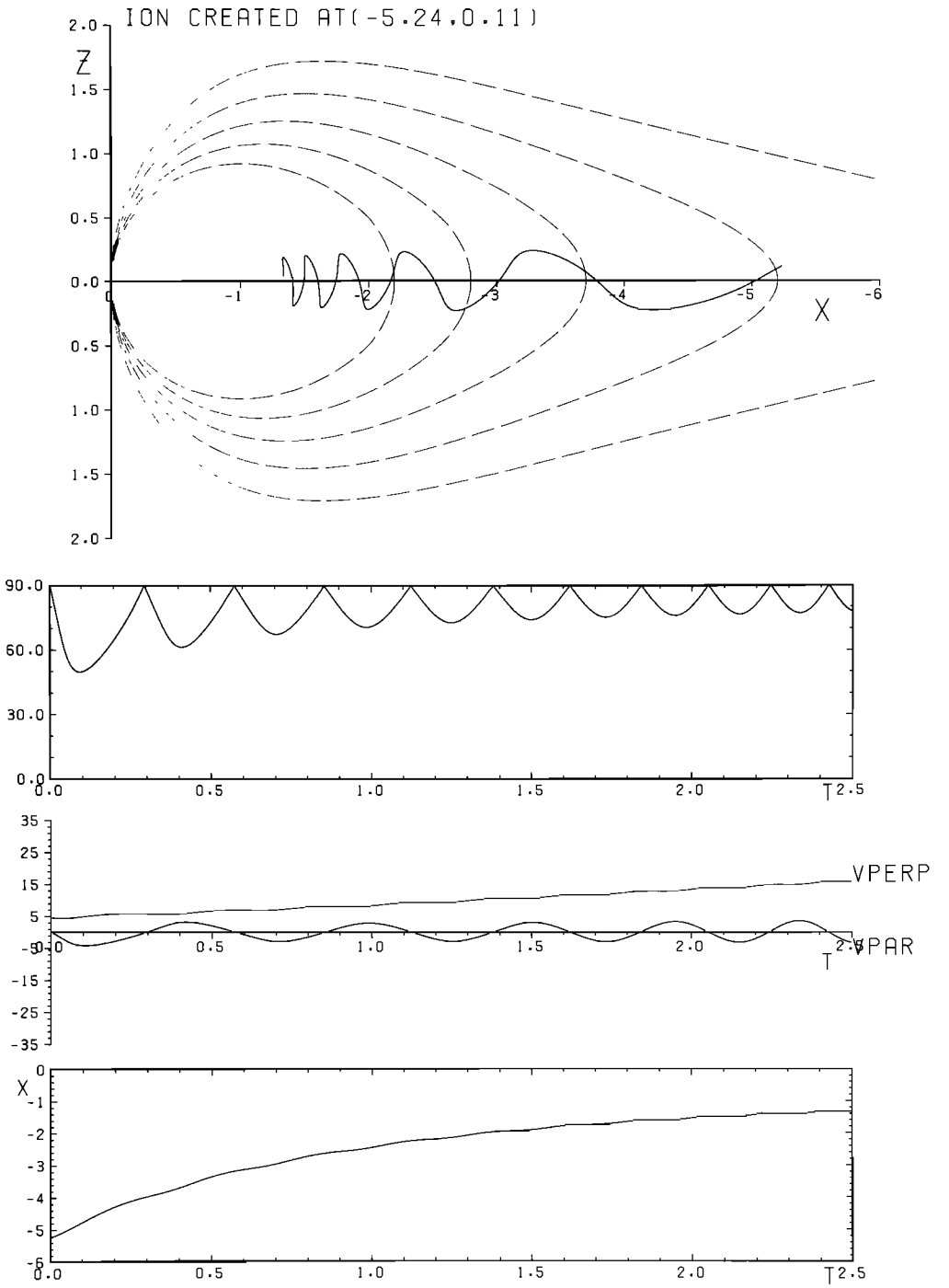

Fig. 4. Plots of the trajectory, pitch angle and velocity components in the same format as Figure 3 for an ion created at $z^* = 0.11$ (i.e., $z \simeq 0.42\ R_E$) at a down-tail distance of 20 R_E, such that at the point of creation $B_x \simeq B_z/2$.

motion along and around the field lines is small on the time scale Ω_i^{-1}, where Ω_i is the ion gyrofrequency. Suitable dimensionless smallness parameters associated with $v_{\parallel}$ and $v_{\perp}$ can be shown to be

$$\varepsilon_{\parallel} = \frac{v_{\parallel}}{\Omega_i} \frac{|(\underline{B}\cdot\underline{\nabla})\underline{B}|}{B^2} \qquad \varepsilon_{\perp} = \frac{v_{\perp}}{\Omega_i} \sum_j \frac{|\underline{B}\wedge\underline{\nabla}\, B_j|}{B^2}$$

and these were computed along the trajectories to ensure that large values did not occur. As may be anticipated, for the majority of ions created away from the immediate vicinity of the sheet center whose equatorial pitch angles are small, the largest values occur in $\varepsilon_{\parallel}$ at each crossing of the center plane. The largest absolute value of $\varepsilon_{\parallel}$ occurs at the first crossing, values at subsequent crossings becoming successively smaller. At the

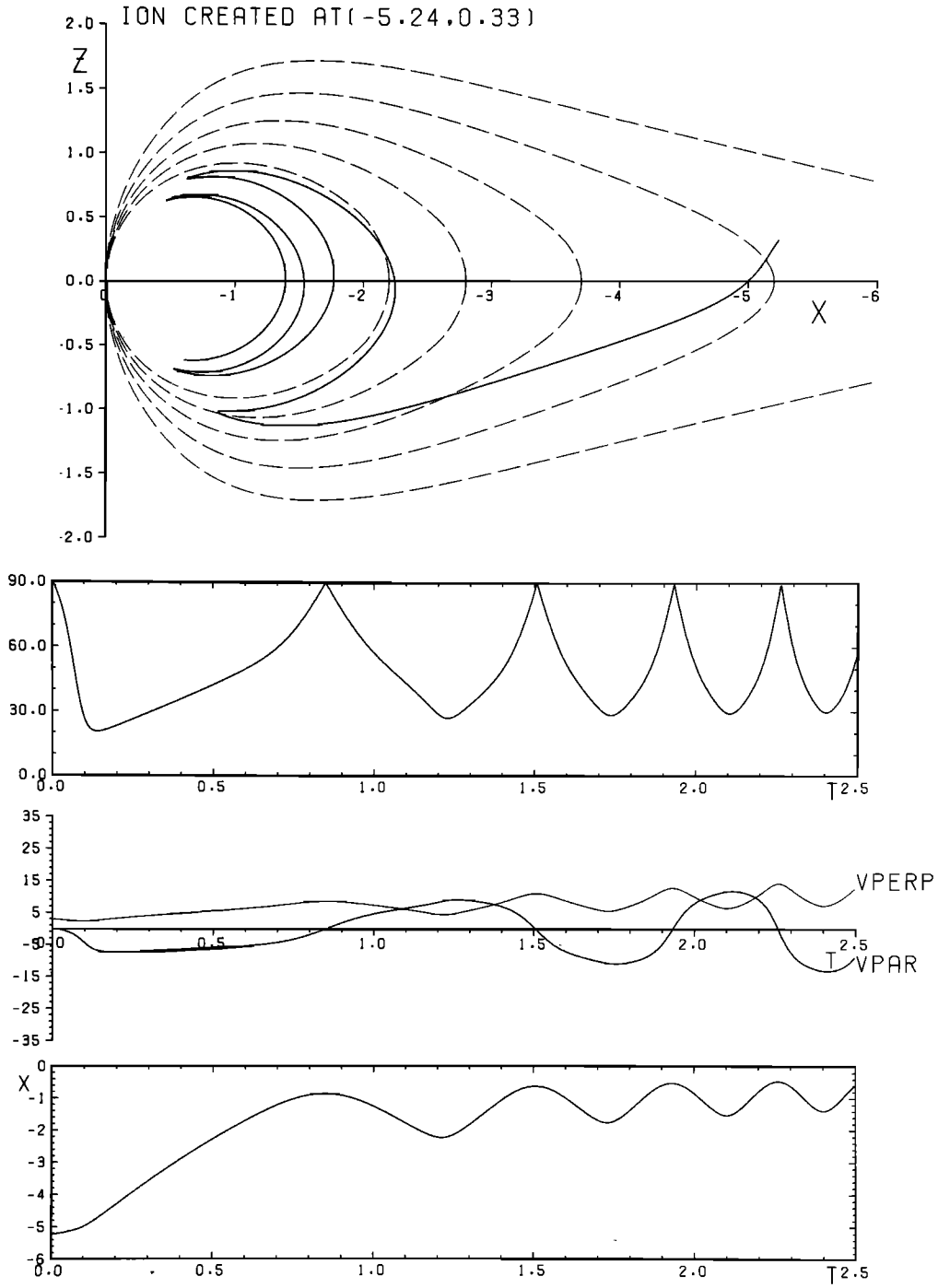

Fig. 5. Plots of the trajectory, pitch angle and velocity components in the same format as Figure 3 for an ion created at $z^* = 0.33$ (i.e., $z \simeq 1.28\ R_E$) at a down-tail distance of 20 R_E, such that at the point of creation $B_x \simeq 1.5\ R_E$.

first crossing $|v_{\shortparallel}| \simeq E_y/B_z$, so that the maximum value of $\epsilon_{\shortparallel}$ on these trajectories is approximately

$$\epsilon_{\shortparallel} \simeq \left(\frac{E_y}{\Omega_{i_z} B_z}\right)\left(\frac{1}{B_z}\frac{dB_x}{dz}\bigg|_{z=0}\right)$$

It can be seen that for a given magnetic field model a limitation on $\epsilon_{\shortparallel}$ corresponds to a limitation on the cross-tail electric field E_y. From section 3 it will be recalled that the guiding center trajectories themselves are independent of E_y, but that the rate at which they are traced out (and hence the rate at which the field changes at the particle) is proportional to E_y. To estimate the maximum value of $\epsilon_{\shortparallel}$ permissible before non-adiabatic pitch angle scattering in the current sheet becomes important we have integrated the exact equations of motion for particles in a simple one-dimensional current sheet. These results indicate that the pitch angle scattering is acceptably small for $\epsilon_{\shortparallel} \lesssim 0.25$, but becomes rapidly large thereafter. For lithium ions in the model

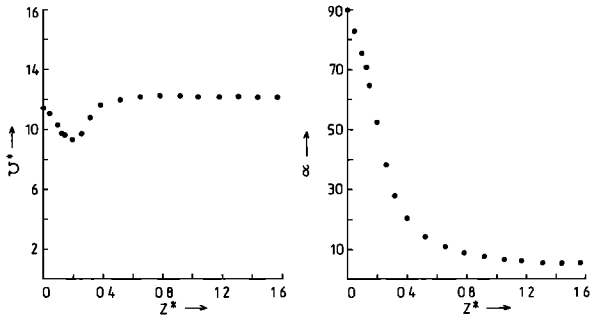

Fig. 6. The normalized speed v* and equatorial pitch angle α of ions on crossing a specific ring current field line (which intersects the center plane at x = − 8 R_E, or x* ≃ − 2.09) plotted versus the height z* above the current sheet center at which they were created at x = − 20 R_E. The equatorial pitch angle was calculated from local velocity values on crossing this field line by transforming at constant energy and μ.

field at x ≃ − 18.8 R_E where, e.g., the particle in Figure 3 first crosses z = 0 we have $B_z \simeq 4.3$ nT and $dB_x/dz|_{z=0} \simeq 4.7$ nT R_E^{-1}, so that the corresponding limitation on E_y is $E_y \lesssim 0.4$ mV m^{-1}. This electric field, if uniform, corresponds to a cross-tail voltage of ∿100 kV which is generally rather large compared with values typical of the quiet time magnetosphere [e.g., Reiff et al., 1981]. The guiding center approximation should thus be adequate for the field model used here for more typical $E_y \simeq 0.2$ mV m^{-1} values. This conclusion is found to remain valid when the larger pitch angle ions created near the plasma sheet center are also considered.

The other approximation used here is that the initial ∿ 4 km s^{-1} "thermal" speed of the parent atoms can be neglected in comparison with the electric drift speeds in the tail. Clearly this assumption will only have an important effect on the qualitative nature of the results if the equatorial field line speed U_{E_C} at the first current sheet encounter becomes comparable with or smaller than the thermal speed. For our model magnetic field this sets a lower limit on the electric field of $E_y \gtrsim 0.04$ mV m^{-1} (so that U_{E_C} exceeds ∿ 10 km s^{-1} for $B_z \simeq 4$ nT), corresponding to a cross-tail voltage of ∿ 10 kV. In summary therefore, our approximations should remain valid over the range of cross-tail voltages from ∿ 10 to ∿ 100 kV, thus spanning the range of usual quiet time values.

5. Conclusions

In this paper we have used the guiding center approximation to integrate the trajectories of lithium test ions as they convect earthward from their release point ∿ 20 R_E down the tail into the quasi-dipolar ring current region, using a simple two-dimensional model of the quiet time nightside magnetosphere. It has been found that the energy of the ions arriving in the ring current region depends principally on the $\underline{E} \wedge \underline{B}$ drift speed at the equator ($U_{E_C} \simeq E_y/B_z$) at the distance of the release, but does not depend substantially on the distance from the center of the plasma sheet where the ions are created. Estimates of the expected energy in the ring current region are of the order of 500 eV to ∿ 1 keV. However, the velocity component in which this energy appears does depend on where the ion is created relative to the sheet center. For ions created very close to the center plane where $B_z \gtrsim |B_x|$ the important component is $v_\perp$ and the pitch angles are correspondingly large. The majority of ions created away from the center plane where $|B_x| > B_z$, however, are accelerated in $v_{||}$ rather than in $v_\perp$ as they cross the current sheet center, and they subsequently convect into the ring current region with small pitch angles typically in the range ∿ 5° − 15°. These results therefore suggest that the lithium ions to be released by the AMPTE IRM spacecraft in the tail will be subsequently detected by the CCE spacecraft in the outer ring current region predominantly as a ∿ 500-eV to ∿ 1-keV field-aligned (∿ 5° to 20°) beam.

Acknowledgements. This work was performed while one of the authors (S.C.C.) was supported by a UK SERC Studentship.

The editor thanks L. Lyons and D. Beard for their assistance in evaluating this paper.

References

Behannon, K. W., Mapping of earth's bow shock and magnetic tail by Explorer 33, J. Geophys. Res., 73, 907, 1968.

Behannon, K. W., Geometry of the geomagnetic tail, J. Geophys. Res., 75, 743, 1970.

Cowley, S. W. H., Plasma populations in a simple open model magnetosphere, Space Sci. Rev., 26, 217, 1980.

de Hoffman, F., and E. Teller, Magneto-hydrodynamic shocks, Phys. Rev., 80, 692, 1950.

Fairfield, D. H., On the average configuration of the geomagnetic tail, J. Geophys. Res., 84, 1950, 1979.

Krimigis, S. M., G. Haerendel, R. W. McEntire, G. Paschmann, and D. A. Bryant, The Active Magnetospheric Particle Tracer Explorers (AMPTE) program, Eos Trans. AGU, 63, 843, 1982.

Mihalov, J. D., D. S. Colburn, R. G. Currie, and C. P. Sonnett, Configuration and reconnection of the geomagnetic tail, J. Geophys. Res., 73, 943, 1968.

Northrop, T. G., The adiabatic motion of charged particles, Wiley Interscience, New York, 1963.

Reiff, P. H., R. W. Spiro, and T. W. Hill, Dependence of polar cap potential drop on interplanetary parameters, J. Geophys. Res., 86, 7639, 1981.

Speiser, T. W., Particle trajectories in model current sheets, J. Geophys. Res., 70, 4219, 1965.

S. C. Chapman and S. W. H. Cowley, The Blackett Laboratory, Imperial College of Science and Technology, London SW7 2BZ, United Kingdom.

(Received February 6, 1984;
revised March 23, 1984;
accepted March 26, 1984.)